Melting Experiments on Fe-O-H: Evidence for Eutectic Melting in Fe-FeH and Implications for Hydrogen in the Core

Kenta Oka[1], Shoh Tagawa[1,2], Kei Hirose[1,2], and Yasuo Ohishi[3]

[1]Department of Earth and Planetary Science, The University of Tokyo, Bunkyo, Tokyo, Japan
[2]Earth-Life Science Institute, Tokyo Institute of Technology, Meguro, Tokyo, Japan
[3]Japan Synchrotron Radiation Research Institute, SPring-8, Sayo, Hyogo, Japan

Key Points:

- We examined the liquidus phase relations and solid/liquid partitioning in the Fe-O±H system at ~40 GPa and ~150 GPa.
- Eutectic melting between Fe and FeH is indicated from the liquidus phase relations in Fe-O-H and the subsolidus phase equilibria in Fe-H.
- The outer core may include 2.9–5.2 wt% O, 0.03–0.32 wt% H, 0–3.4 wt% Si, and 1.7 wt% S.

Abstract We examined liquidus phase relations in Fe-O±H at ~40 and ~150 GPa, and subsolidus phase equilibria in Fe-FeH. While it has been speculated that Fe and FeH form continuous solid solution to core pressures, our experiments show the coexistence of the H-poor hcp and H-rich fcc phases in the Fe-FeH system. Considering higher melting temperature of stoichiometric FeH than that of Fe-FeH, it indicates eutectic melting between Fe and FeH. It is consistent with the liquidus phase diagram in Fe-O-H, which implies the Fe-FeH binary eutectic liquid composition of $FeH_{0.42}$ at ~40 GPa. We estimated the outer core liquid composition to be Fe + 2.9–5.2% O + 0.03–0.32% H + 0–3.4% Si + 1.7% S by weight, based on the liquidus phase relations, solid-liquid partitioning, and outer/inner core densities and velocities, indicating that O and either H or Si are important core light elements.

Plain Language Summary We have investigated the liquidus and subsolidus phase relations in the Fe-O±H and Fe-H systems, respectively, at high pressures in a laser-heated diamond-anvil cell. The solid-liquid partition coefficient of H was also determined. While it is known that Fe and stoichiometric FeH form continuous solid solution at least to ~20 GPa, our experiments on the Fe-O-H ternary and Fe-H binary systems performed above 40 GPa consistently suggested eutectic melting between Fe and FeH with eutectic liquid

composition of $FeH_{0.42}$. We explored the possible range of the liquid core composition, which should be 1) within the liquidus field of Fe to crystallize the dense inner core, 2) compatible with seismological observations of the outer core, and 3) in equilibrium with the inner core solid that explains the observed density and velocities. The results indicate that the outer core is rich in O and either H or Si, supporting the delivery of a large amount of water to the Earth found in recent planet formation theories and its sequestration into the metallic core that is inferred from metal-silicate partitioning data.

1. Introduction

The Earth's core should contain more than one light impurity elements (see recent reviews by Li & Fei, 2014 and Hirose et al., 2021). Both O and H can be important core light elements because the density and sound velocity observed in the outer core are compatible with the presence of O (Badro et al., 2014) and H (Umemoto & Hirose, 2015, 2020). Recent planet formation models suggested that 10 to 100 times ocean mass of water may have been brought to the Earth during its accretion (e.g., Raymond et al., 2007; Walsh et al., 2011). The chemical reaction of solar-nebula-type H-rich proto-atmosphere with FeO could have been another source of water (Ikoma & Genda, 2006; Olson & Sharp, 2019). It is likely that most of H_2O was once dissolved into a magma ocean, and H and O were incorporated into core-forming metals during their segregation from silicate (Tagawa, Sakamoto et al., 2021; Li et al., 2020; Yuan & Steinle-Neumann, 2020).

Liquidus phase relations of Fe alloy systems, in particular the liquidus field of Fe (a compositional range of liquids that first crystallize Fe), constrain the outer core composition (e.g., Yokoo et al., 2019; Hasegawa et al., 2021). When O and H are two major core light elements, the liquid core should not crystallize FeO nor FeH but Fe at the inner core boundary (ICB), otherwise the denser solid inner core is not formed. In order to understand the liquidus phase relations in the Fe-O-H system, the knowledge on the relevant binary systems is helpful. Previous high-pressure experiments demonstrated that O concentration in the Fe-FeO eutectic liquid increases with increasing pressure (Morard et al., 2017; Oka et al., 2019). The recent study by Oka and others based on experiments to 204 GPa estimated 15 wt% O in the Fe-FeO binary eutectic liquid at ICB. On the other hand, earlier high-pressure melting experiments on the Fe(±Ni)-H system were limited to 20 GPa (Sakamaki et al., 2009; Imai, 2013; Shibazaki et al., 2014) because of a technical difficulty in dealing with hydrogen. Fukai (1992) speculated a continuous solid solution between Fe and stoichiometric FeH to megabar pressure, but it has been verified only to ~20 GPa (Imai, 2013; Shibazaki et al., 2014).

In this study, we have carried out melting experiments on the Fe-O±H system at ~40 GPa and ~150 GPa. Our results on Fe-O-H suggest that Fe-FeH is an eutectic system, which contradicts the phase diagram supposed by Fukai (1992) but is supported by our additional experiment on an Fe-H alloy. Our findings of 1) eutectic melting between Fe and FeH, 2) liquidus phase relations in the Fe-O-H system, and 3) the solid-liquid partitioning of H help to constrain concentrations of O, H, and other light elements in the outer core.

2. Results

We have examined the phase relations in the Fe-O±H and Fe-FeH systems on the basis of high-pressure and -temperature (*P*-*T*) experiments using laser-heated diamond-anvil cell (DAC) techniques, combined with in-situ synchrotron X-ray diffraction (XRD) measurements and ex-situ textural and compositional characterizations using electron microprobes (see Experimental Methods in the Supporting Information).

2.1. Melting in Fe-O±H

A total of six separate melting experiments were carried out at ~40 GPa and ~150 GPa (runs #A1–A6 in Table S1). For all runs, we performed synchrotron XRD measurements and subsequent microprobe observations on recovered samples. In run #A4, while the intense peaks from hcp Fe were present before heating, they were almost lost and alternatively a diffuse signal characteristic of liquid was observed around 12 degrees of two-theta angle upon heating to 2370 K (Figure 1a). Upon quenching temperature, the peaks of fcc FeH_x (x = 0.31) appeared from liquid. The XRD pattern obtained at ~12 μm away from the center of a laser-heated spot included strong peaks from rhombohedrally-distorted B1 FeO and hcp FeH_x (x = 0.24).

This sample was recovered from a DAC, and in its cross section, there was a chemically homogeneous area with a non-stoichiometric composition at the center, which represents a quenched liquid (Figures 2a, b). The earlier DAC experiments by Hirose et al. (2019) and Tagawa, Sakamoto et al. (2021) demonstrated that the H content in FeH_x crystals formed from liquid upon quenching temperature closely represents that of Fe-H liquid. We therefore consider that Fe-O-H liquids in the present experiments were fully quenched into a mixture of solid FeH_x and FeO. The proportion of FeO was obtained from the EPMA analysis of O concentration in the quenched liquid. The remaining phase proportion of FeH_x and its H concentration x that was estimated from its lattice volume in XRD patterns give 0.49 wt% H in the Fe-O-H liquid (Table S1). Next to the liquid pool,

electron microprobe images showed a couple of single-phase layers of Fe and FeO (Figures 2a, b). According to the XRD observations, the Fe layer was solid $FeH_{0.24}$ (Fe + 0.43 wt% H) before it lost hydrogen during decompression (Figure 1a). The liquid was in direct contact with the FeO layer or in some place with the $FeH_{0.24}$ layer, indicating that both FeO and $FeH_{0.24}$ are the liquidus phases of the Fe-O-H liquid formed in run #A4. The outside of these liquidus phase layers was not melted during laser heating. Runs #A1–A3 were carried out around 40 GPa in a similar manner with changing the Fe/H_2O ratio in the starting materials (Table S1). The liquids included 0.1–0.4 wt% C except 1.7 wt% C in run #A1.

In runs #A5 and #A6 performed at ~150 GPa, liquids were crystallized into the hcp phase upon quenching temperature to 300 K, which included minimal amounts of H (<0.04 wt%) (Table S1). The EPMA data showed 10.4–13.0 wt% O and 0.9–3.7 wt% C in quenched liquids, indicating they were Fe-O±C liquids. The liquid Fe-13.0wt%O-0.9wt%C obtained in run #A5 coexisted with solid Fe, giving the lower bound for O concentration in the Fe-FeO binary eutectic liquid at 147 GPa (Figure S1). It helps to constrain the change in the eutectic liquid composition in the Fe-FeO system with increasing pressure, which was previously estimated only with a single datum point above 50 GPa in Oka et al. (2019).

2.2. Subsolidus Phase Relations in Fe-FeH

An additional experiment was carried out on the Fe-FeH binary system at 62 GPa (run #B in Table S2) (see Experimental Methods in the Supporting Information). Stoichiometric dhcp FeH was synthesized by heating to <1000 K at 8 GPa. The excess molecular H_2 in the sample chamber was lost to a neighboring rhenium gasket to form ReH_x upon compression to 23 GPa (Scheler et al., 2011). The dhcp FeH was then transformed into fcc $FeH_{0.87}$ by reheating to ~1000 K for 3 min at 44 GPa (Figure 1b). Subsequently this sample was further compressed to ~60 GPa and reheated for ~40 min at each temperature. At 1640 K and 62 GPa, while the sample was still fcc FeH_x, its H content x reduced from 0.87 to 0.77. At higher temperature of 1830 K, it further diminished to 0.69, and at the same time hcp $FeH_{0.21}$ appeared. The sample melted at a slightly higher temperature.

3. Discussion

3.1. Eutectic Melting in Fe-FeH and the Liquidus Phase Relations in Fe-O-H

The high-pressure phase relations in the Fe-H system have been speculated by Fukai (1992), suggesting 1) a continuous solid solution between Fe and FeH and 2) an eutectic point located at FeH_x ($x > 1$). The multi-anvil experiments by Imai (2013) and Shibazaki et al. (2014) reported the melting and subsolidus phase relations in the Fe-FeH(±Ni) system to 15–20 GPa, which are consistent with the phase diagram supposed by Fukai (1992). In contrast, run #B in the present study demonstrated the coexistence of hcp $FeH_{0.21}$ and fcc $FeH_{0.69}$ at 62 GPa and 1830 K (Figure 1b), indicating a gap in solid solution right below the melting temperature. In addition, earlier experiments demonstrated that stoichiometric FeH does not melt, at least to 2600 K at this pressure (Tagawa, Gomi et al., 2021). These suggest eutectic (not peritectic) melting between the H-poor hcp and H-rich fcc phases in the Fe-FeH system. Indeed, the eutectic melting is a natural consequence of the facts that 1) Fe and FeH end-members adopt different crystal structures of hcp (Komabayashi et al., 2009) and fcc (Kato et al., 2020; Thompson et al., 2018; Isaev et al., 2007), respectively and 2) stoichiometric FeH melts at temperature much higher than that for $FeH_{0.21–0.69}$. The presence of the gap in solid solution between hcp Fe and fcc FeH and the resulting eutectic melting are likely to be hold to Earth's inner core conditions (Tagawa, Gomi et al., 2021).

The compositions of liquids obtained at ~40 GPa in runs #A1–A4 are plotted in the Fe-O-H ternary diagram (Figure 3a). The liquid compositions found in runs #A2 and #A3 should be within the liquidus field of FeO, and that in run #A4 is on the Fe + FeO cotectic line (showing the liquid compositions coexisting with both Fe and FeO). Considering the eutectic point in the Fe-FeO binary (Figure S1), the position of the Fe + FeO cotectic line is tightly constrained. Figure 3a illustrates the liquidus phase relations in the Fe-O-H system. The liquidus field of FeO extends close to the Fe-FeH side, and the ternary peritectic (or possibly eutectic) point should be located at the H-rich portion of the phase diagram. It suggests the presence of the Fe-FeH binary eutectic point at $FeH_{0.42}$ (Fe + 0.75 wt% H) in agreement with a gap in solid solution between hcp $FeH_{0.21}$ and fcc $FeH_{0.69}$ right below the melting temperature as observed in run #B.

The Fe-FeH binary eutectic liquid composition may change little with increasing pressure because the high *P-T* experiments performed by Tagawa, Gomi et al. (2021) showed that the temperature/pressure slope of the melting curve of stoichiometric FeH could be similar to that of Fe at >40 GPa. On the other hand, the present results on the Fe-FeO system as well as earlier experiments (Seagle et al., 2008; Oka et al., 2019) and thermodynamic calculations (Komabayashi, 2014) demonstrate that O concentration in the Fe-FeO binary eutectic liquid increases to 15 wt% with increasing pressure to 330

GPa. The Fe-O±C liquids obtained in runs #A5 and #A6 verify the pressure evolution of the Fe-FeO eutectic liquid composition (the composition of liquid that coexists with both Fe and FeO) in the presence of <1 wt% and ~3 wt% C, respectively (Figure S1). By taking the positions of the Fe-FeO and Fe-FeH binary eutectic points into account, we suppose the Fe-O-H ternary liquidus phase relations at the ICB pressure in Figure 3b.

3.2. Possible Outer Core Liquid Composition

Since the outer core crystallizes the dense inner core at the ICB, the liquid composition should be within the liquidus field of Fe at 330 GPa (Figure 3b). It has been demonstrated by earlier experiments on ternary Fe alloy systems containing two light elements—Fe-Si-S (Tateno et al., 2018), Fe-S-O (Yokoo et al., 2019), Fe-Si-C (Hasegawa et al., 2021), and Fe-C-O (Sakai et al., 2021)—that the ternary eutectic point is located close to the tie line between the eutectic points in relevant binary systems; in other words, the liquidus field of Fe (such as a colored area in Figure 3b) in these ternary systems can be approximated by linear interpolation between the eutectic liquid compositions in relevant binary systems. This may be extended to the Fe-O-H-Si-S system that we consider for the liquid outer core; the liquidus field of Fe could be estimated from the four relevant binary eutectic compositions at 330 GPa; Fe with 15 wt% O (Figure S1), 0.75 wt% H (Figure 3b), 8 wt% Si (Hasegawa et al., 2021), or 5 wt% S (Mori et al., 2017).

We estimate the possible range of the outer core liquid composition based on three independent constraints (Hirose et al., 2021). First, 1) it must account for the density and P-wave velocity observed in the outer core (Umemoto & Hirose, 2020). Here we consider T_{ICB} = 5800 K and 6280 K, which correspond to T_{360GPa} = 6000 K and 6500 K, respectively, when assuming isentropic temperature profiles with Grüneisen parameter γ = 1.5 (Vočadlo et al., 2003) (these are the conditions at which the possible inner core composition was examined by Wang et al., 2021). Also, 2) the liquid core composition should be within the liquidus field of Fe in the Fe-O-H-Si±1.7wt%S system at the ICB pressure. Geochemical and cosmochemical estimates have consistently proposed ~2 wt% S in the core (Dreibus & Palme, 1996; McDonough, 2014), and here we adopt 0 or 1.7 wt% S in the outer core according to Dreibus & Palme. The colored portions in Figures 4a–d indicate O, H, and Si concentrations in liquids Fe-O-H-Si±1.7wt%S, which meet these two constraints from 1) the outer core density and velocity and 2) the liquidus phase diagram at 330 GPa.

In addition, 3) the third constraint is from the possible inner core solid composition that was estimated in Fe-Si-S(-C) by Li et al. (2018) and in Fe-H-Si by Wang et al. (2021),

which explains the observed density, P-wave and S-wave velocities (Dziewonski & Anderson, 1981; Kennett et al., 1995). Their calculations of $Fe_{64-y}Si_y$ (y = 0, 4, and 8) and $Fe_{60}Si_4H_z$ (z = 1, 2, 4, and 8) alloys demonstrated that the density (ρ), P-wave (V_P) and S-wave velocities (V_S) of Fe alloys are written as; $\rho = -0.105y - 0.039z + 13.639(5)$, $V_P = -0.001y - 0.034z + 11.559(128)$, and $V_S = -0.061y - 0.053z + 4.108(154)$ at T_{360GPa} = 6500 K, and $\rho = -0.104y - 0.038z + 13.682(48)$, $V_P = 0.001y - 0.019z + 11.619(110)$, and $V_S = -0.060y - 0.033z + 4.229(140)$ at T_{360GPa} = 6000 K. The inner core may include 1.4 wt% S, which is calculated from the 1.7 wt% S in the outer core and the solid/liquid partition coefficient of S, D_S (solid/liquid) = 0.8 by weight at 330 GPa (Alfè et al., 2002; Yokoo et al., 2019). Since Wang et al. (2021) mentioned that the effects of S and Si on the density and sound velocities are similar to each other, we consider that the effect of S is the same as that of Si. O is not partitioned into solid Fe and thus not considered in the inner core (Alfè et al., 2002; Ozawa et al., 2010). With these relations, we obtain the possible ranges of the inner core composition in the Fe-H-Si±1.4wt%S system, depending on temperature. It gives the liquid outer core composition based on the solid/liquid partition coefficients D_H = 0.89 (this study, Table S1) and D_{Si} (solid/liquid) = 1.0 by weight (Alfè et al., 2002; Kuwayama & Hirose, 2004). The D_H = 0.89 obtained in this study at 39 GPa is slightly higher than 0.72–0.74 reported by earlier multi-anvil experiments at 15–20 GPa (Imai, 2013). The compositional ranges of liquids in equilibrium with the possible inner core solid are illustrated by areas enclosed by black lines in Figures 4a–d.

The overlap between the colored area (constrained by the outer core density and velocity and by the liquidus field of Fe) and the black enclosed area (constrained by the inner core density and velocities) in Figures 4a–d indicates the possible compositional range for the liquid outer core. It becomes smaller with 1.7 and 1.4 wt% S respectively in the outer and inner core than in S-free cases. Possible liquid compositions are not found in the Fe-O-H-Si-1.7wt%S system when T_{ICB} = 5800 K (T_{360GPa} = 6000 K) (Figure 4c). If T_{ICB} = 6280 K (T_{360GPa} = 6500 K), the outer core may include 2.9–5.2 wt% O, 0.03–0.32 wt% H, and 0–3.4 wt% Si and in addition to 1.7 wt% S. It suggests that O and either H or Si are important light elements in the core, supporting the recent arguments that a large amount of water was brought to the Earth during its accretion and mostly incorporated into core-forming metals (Tagawa, Sakamoto et al., 2021; Li et al., 2020; Yuan & Steinle-Neumann, 2020). The range of the O content is still consistent with the recent estimate of <3.8 wt% O in the outer core to explain the density jump across the ICB, which was based on the experimentally-determined equations of state of liquid and solid Fe (Kuwayama et al., 2020). Indeed, ~0.2 wt.% C could be also present in the core (Fischer et al., 2020), but it hardly decreases the present estimates of the core inventories of other light elements.

The T_{ICB} = 6280 K (T_{360GPa} = 6500 K), however, corresponds to about 4600 K at the CMB when γ = 1.5 (Vočadlo et al., 2003). It is much higher than the solidus temperatures of the pyrolitic and chondritic mantle materials at 135 GPa (Fiquet et al., 2010; Andrault et al., 2011; Nomura et al., 2014; Kim et al., 2020). It could therefore lead to extensive melting in the lowermost mantle, but seismology reveals the presence of partial melts only locally above the CMB at ultralow velocity zones. It is necessary to better constrain the core temperature to further explore the possible core composition (Hirose et al., 2021).

4. Conclusions

We obtained the liquidus phase relations in the Fe-O-H ternary system at ~40 GPa based on melting and subsolidus experiments on Fe-O±H and Fe-H, respectively. While earlier studies reported that Fe and stoichiometric FeH form a continuous solid solution below ~20 GPa (Sakamaki et al., 2009; Imai, 2013; Shibazaki et al., 2014), our results indicated eutectic melting between Fe and FeH from the observations that 1) hcp Fe coexists with fcc FeH right below melting temperature, 2) stoichiometric FeH melts at temperature much higher than the melting temperature of $FeH_{0.21–0.69}$ (Tagawa, Gomi et al., 2021), and 3) melting phase relations in the Fe-O-H ternary require the eutectic point in the Fe-FeH system. The Fe-FeH eutectic liquid composition is found to be $FeH_{0.42}$ (Fe + 0.75 wt% H) at ~40 GPa. The present study combined with earlier experiments demonstrates that O concentration in the Fe-FeO binary eutectic liquid increases to 15 wt% at 330 GPa. On the other hand, pressure effect on the Fe-FeH eutectic liquid composition is likely small because the temperature/pressure slope of FeH may be comparable to that of Fe (Tagawa, Gomi et al., 2021). These allow us to extrapolate the liquidus phase relations in the Fe-O-H system to 330 GPa.

We estimated the possible range of the outer core liquid composition to be Fe + 2.9–5.2 wt% O + 0–3.4 wt% Si + 0.03–0.32 wt% H + 1.7 wt% S, based on constraints from 1) the liquidus field of Fe (in order to crystallize the dense inner core), 2) the outer core density and velocity, and 3) the inner core density and velocities (the outer core composition is calculated from that of the inner core using the solid-liquid partition coefficients of light elements at ICB conditions). It indicates that O and either H or Si are important core light impurity elements, which supports recent arguments on the delivery of a large amount of water to the growing Earth and its incorporation into core metals for the most part.

Data Availability Statement

Datasets for this research are found in Tables S1 and S2 available online (from https://doi.org/10.5281/zenodo.5906236).

Acknowledgments

We thank K. Yonemitsu for sample analyses with FIB, EDS, and FE-EPMA. This work was supported by the JSPS research grants 16H06285 and 21H04506 to K.H. XRD measurements were performed at BL10XU, SPring-8 (proposals no. 2016B0072, 2019A0072, and 2019B0072).

References

Alfè, D., Gillan, M. J., & Price, G. D. (2002). Composition and temperature of the earth's core constrained by combining ab initio calculations and seismic data. *Earth and Planetary Science Letters*, *195*, 91–98. https://doi.org/10.1016/S0012-821X(01)00568-4

Andrault, D., Bolfan-Casanova, N., Nigro, G. Lo, Bouhifd, M. A., Garbarino, G., & Mezouar, M. (2011). Solidus and liquidus profiles of chondritic mantle: implication for melting of the Earth across its history. *Earth and Planetary Science Letters*, *304*, 251–259. https://doi.org/10.1016/j.epsl.2011.02.006

Badro, J., Cote, A. S., & Brodholt, J. P. (2014). A seismologically consistent compositional model of Earth's core. *Proceedings of the National Academy of Science of the United States of America*, *111*, 7542–7545. https://doi.org/10.1073/pnas.1316708111

Dreibus, G., & Palme, H. (1996). Cosmochemical constraints on the sulfur content in the Earth's core. *Geochimica et Cosmochimica Acta*, *60*, 1125–1130. https://doi.org/10.1016/0016-7037(96)00028-2

Dziewonski, A. M., & Anderson, D. L. (1981). Preliminary reference Earth model. *Physics of the Earth and Planetary Interiors*, *25*, 297–356. https://doi.org/10.1016/0031-9201(81)90046-7

Fukai, Y. (1992). Some properties of the Fe-H system at high pressures and temperatures, and their implications for the Earth's core. In Y. Syono, M.H. Manghnani (Eds.), *High-pressure research: applications to Earth and planetary sciences* (Vol. 67, pp. 373–385). https://doi.org/10.1029/GM067p0373

Fischer, R. A., Cottrell, E., Hauri, E., Lee, K. K. M., & Le Voyer, M. (2020). The carbon content of Earth and its core. *Proceedings of the National Academy of Sciences of the*

United States of America, *117*, 8743–8749. https://doi.org/10.1073/pnas.1919930117

Fiquet, G., Auzende, A. L., Siebert, J., Corgne, A., Bureau, H., Ozawa, H., & Garbarino, G. (2010). Melting of peridotite to 140 gigapascals. *Science*, *329*, 1516–1518. https://doi.org/10.1126/science.1192448

Hasegawa, M., Hirose, K., Oka, K., & Ohishi, Y. (2021). Liquidus phase relations and solid-liquid partitioning in the Fe-Si-C system under core pressures. *Geophysical Research Letters*, *48*, e2021GL092681. https://doi.org/10.1029/2021GL092681

Hirose, K., Wood, B., & Vočadlo, L. (2021). Light elements in the Earth's core. *Nature Reviews Earth & Environment*, *2*, 645–658. https://doi.org/10.1038/s43017-021-00203-6

Ikoma, M., & Genda, H. (2006). Constraints on the mass of a habitable planet with water of nebular origin. *The Astrophysical Journal*, *648*, 696. https://doi.org/10.1086/505780

Imai, T. (2013). *Crystal/melt partitioning under deep mantle conditions and melting phase relation in the system Fe-FeH* (PhD thesis). Tokyo Institute of Technology

Isaev, E. I., Skorodumova, N. V., Ahuja, R., Vekilov, Y. K., & Johansson, B. (2007). Dynamical stability of Fe-H in the Earth's mantle and core regions, *Proceedings of the National Academy of Sciences of the United States of America*, *104*, 9168–9171. https://doi.org/10.1073/pnas.0609701104

Kato, C., Umemoto, K., Ohta, K., Tagawa, S., Hirose, K., & Ohishi, Y. (2020). Stability of fcc phase FeH to 137 GPa. *American Mineralogist*, *105*, 917–921. https://doi.org/10.2138/am-2020-7153

Kennett, B. L. N., Engdahl, E. R., & Buland, R. (1995). Constraints on seismic velocities in the Earth from traveltimes. *Geophysical Journal International*, *122*, 108–124. https://doi.org/10.1111/j.1365-246X.1995.tb03540.x

Kim, T., Ko, B., Greenberg, E., Prakapenka, V., Shim, S. H., & Lee, Y. (2020). Low melting temperature of anhydrous mantle materials at the core-mantle boundary. *Geophysical Research Letter*s, *47*, 1–10. https://doi.org/10.1029/2020GL089345

Komabayashi, T. (2014). Thermodynamics of melting relations in the system Fe-FeO at high pressure: implications for oxygen in the Earth's core. *Journal of Geophysical Research: Solid Earth*, *119*, 4164–4177. https://doi.org/10.1002/2014JB010980

Komabayashi, T., Fei, Y., Meng, Y., & Prakapenka, V. (2009). In-situ X-ray diffraction measurements of the γ-ε transition boundary of iron in an internally-heated diamond anvil cell. *Earth and Planetary Science Letters*, *282*, 252–257. https://doi.org/10.1016/j.epsl.2009.03.025

Kuwayama, Y., & Hirose, K. (2004). Phase relations in the system Fe-FeSi at 21 GPa. *American Mineralogist*, *89*, 273–276. https://doi.org/10.2138/am-2004-2-303

Kuwayama, Y., Morard, G., Nakajima, Y., Hirose, K., Baron, A. Q. R., Kawaguchi, S. I., et al. (2020). Equation of state of liquid iron under extreme conditions. *Physical Review Letters*, *124*, 165701. https://doi.org/10.1103/PhysRevLett.124.165701

Li, J., & Fei, Y. (2014). Experimental constraints on core composition. In *Treatise on geochemistry* (2nd ed., Vol. 3, pp. 527−557). Amsterdam. Elsevier. https://doi.org/10.1016/b978-0-08-095975-7.00214-x

Li, Y., Vočadlo, & L., Brodholt, J. P. (2018). The elastic properties of hcp-Fe alloys under the conditions of the Earth's inner core. *Earth and Planetary Science Letters*, *493*, 118–127. https://doi.org/10.1016/j.epsl.2018.04.013

Li, Y., Vočadlo, L., Sun, T., & Brodholt, J. P. (2020). The Earth's core as a reservoir of water. *Nature Geoscience*, *13*, 453–458. https://doi.org/10.1038/s41561-020-0578-1

McDonough, W. F. (2014). Compositional model for the Earth's core. In *Treatise on geochemistry* (2nd ed., Vol. 3, pp. 559–577). Amsterdam. Elsevier. https://doi.org/10.1016/B978-0-08-095975-7.00215-1

Morard, G., Andrault, D., Antonangeli, D., Nakajima, Y., Auzende, A. L., Boulard, E., et al. (2017). Fe–FeO and Fe–Fe_3C melting relations at Earth's core–mantle boundary conditions: implications for a volatile-rich or oxygen-rich core. *Earth and Planetary Science Letters*, *473*, 94–103. https://doi.org/10.1016/j.epsl.2017.05.024

Mori, Y., Ozawa, H., Hirose, K., Sinmyo, R., Tateno, S., Morard, G., & Ohishi, Y. (2017). Melting experiments on Fe–Fe_3S system to 254 GPa. *Earth and Planetary Science Letters*, *464*, 135–141. https://doi.org/10.1016/j.epsl.2017.02.021

Nomura, R., Hirose, K., Uesugi, K., Ohishi, Y., Tsuchiyama, A., Miyake, A., & Ueno, Y. (2014). Low core-mantle boundary temperature inferred from the solidus of pyrolite. *Science*, *343*, 522–525. https://doi.org/10.1126/science.1248186

Oka, K., Hirose, K., Tagawa, S., Kidokoro, Y., Nakajima, Y., Kuwayama, Y., et al. (2019). Melting in the Fe-FeO system to 204 GPa: implications for oxygen in Earth's core. *American Mineralogist*, *104*, 1603–1607. https://doi.org/10.2138/am-2019-7081

Olson, P. L., & Sharp, Z.D. (2019). Nebular atmosphere to magma ocean: a model for volatile capture during Earth accretion. *Physics of the Earth and Planetary Interiors*, *294*, 106294. https://doi.org/10.1016/j.pepi.2019.106294

Ozawa, H., Hirose, K., Tateno, S., Sata, N., & Ohishi, Y. (2010). Phase transition boundary between B1 and B8 structures of FeO up to 210GPa. *Physics of the Earth and Planetary Interiors*, *179*, 157–163. https://doi.org/10.1016/j.pepi.2009.11.005

Raymond, S. N., Quinn, T., & Lunine, J. I. (2007). High-resolution simulations of the final assembly of Earth-like planets. 2. Water delivery and planetary habitability. *Astrobiology*, *7*, 66–84. https://doi.org/10.1089/ast.2006.06-0126.

Sakai, F., & Hirose, K. (2021). Melting experiments on the Fe-C-O ternary system under core pressures. JpGU Meeting Abstract

Sakamaki, K., Takahashi, E., Nakajima, Y., Nishihara, Y., Funakoshi, K., Suzuki, T., & Fukai, Y. (2009). Melting phase relation of FeH_X up to 20 GPa: implication for the temperature of the Earth's core. *Physics of the Earth and Planetary Interiors*, *174*, 192–201. https://doi.org/10.1016/j.pepi.2008.05.017

Seagle, C. T., Heinz, D. L., Campbell, A. J., Prakapenka, V. B., & Wanless, S. T. (2008). Melting and thermal expansion in the Fe-FeO system at high pressure. *Earth and Planetary Science Letters*, *265*, 655–665. https://doi.org/10.1016/j.epsl.2007.11.004

Scheler, T., Degtyareva, O., & Gregoryanz, E. (2011). On the effects of high temperature and high pressure on the hydrogen solubility in rhenium. *Journal of Chemical Physics*, *135*, 214501. https://doi.org/10.1063/1.3652863

Shibazaki, Y., Terasaki, H., Ohtani, E., Tateyama, R., Nishida, K., Funakoshi, K., & Higo, Y. (2014). High-pressure and high-temperature phase diagram for $Fe_{0.9}Ni_{0.1}$-H alloy. *Physics of the Earth and Planetary Interiors*, *228*, 192–201. https://doi.org/10.1016/j.pepi.2013.12.013

Stixrude, L. (2012). Structure of iron to 1 Gbar and 40 000 K. *Physical Review Letters*, *108*, 055505. https://doi.org/10.1103/PhysRevLett.108.055505

Tagawa, S., Gomi, H., Hirose, K., & Ohishi, Y. (2021). High-temperature equation of state of FeH: implications for hydrogen in Earth's inner core. *Earth and Space Science Open Archive*. https://doi.org/10.1002/essoar.10508224.1

Tagawa, S., Sakamoto, N., Hirose, K., Yokoo, S., Hernlund, J., Ohishi, Y., & Yurimoto, H. (2021). Experimental evidence for hydrogen incorporation into Earth's core. *Nature Communications*, *12*, 2588. https://doi.org/10.1038/s41467-021-22035-0

Tateno, S., Hirose, K., Sinmyo, R., Morard, G., Hirao, N., & Ohishi, Y. (2018). Melting experiments on Fe–Si–S alloys to core pressures: silicon in the core? *American Mineralogist*, *103*, 742–748. https://doi.org/10.2138/am-2018-6299

Thompson, E. C., Davis, A. H., Bi, W., Zhao, J., Alp, E. E., Zhang, D., et al. (2018). High-pressure geophysical properties of fcc phase FeH_X. *Geochemistry, Geophysics, Geosystems*, *19*, 305–314. https://doi.org/10.1002/2017GC007168

Umemoto, K., & Hirose, K. (2015). Liquid iron-hydrogen alloys at outer core conditions by first-principles calculations. *Geophysical Research Letters*, *42*, 7513–7520. https://doi.org/10.1002/2015GL065899

Umemoto, K., & Hirose, K. (2020). Chemical compositions of the outer core examined by first principles calculations. *Earth and Planetary Science Letters*, *531*, 116009. https://doi.org/10.1016/j.epsl.2019.116009

Vočadlo, L., Alfè, D., Gillan, M. J., & Price, G. D. (2003). The properties of iron under core conditions from first principles calculations. *Physics of the Earth and Planetary Interiors*, *140*, 101–125. https://doi.org/10.1016/j.pepi.2003.08.001

Walsh, K. J., Morbidelli, A., Raymond, S. N., O'brien, D. P., & Mandell, A. M. (2011). A low mass for Mars from Jupiter's early gas-driven migration. *Nature*, *475*, 206–209. https://doi.org/10.1038/nature10201

Wang, W., Li, Y., Brodholt, J. P., Vočadlo, L., Walter, M. J., & Wu, Z. (2021). Strong shear softening induced by superionic hydrogen in Earth's inner core. *Earth and Planetary Science Letters*, *568*, 117014. https://doi.org/10.1016/j.epsl.2021.117014

Yokoo, S., Hirose, K., Sinmyo, R., & Tagawa, S. (2019). Melting experiments on liquidus phase relations in the Fe-S-O ternary system under core pressures. *Geophysical Research Letters*, *46*, 5137–5145. https://doi.org/10.1029/2019GL082277

Yuan, L., & Steinle-Neumann, G. (2020). Strong sequestration of hydrogen into the Earth's core during planetary differentiation. *Geophysical Research Letters*, *47*, e2020GL088303. https://doi.org/10.1029/2020GL088303

References From the Supporting Information

Akahama, Y., & Kawamura, H. (2004). High-pressure Raman spectroscopy of diamond anvils to 250 GPa: method for pressure determination in the multimegabar pressure range. *Journal of Applied Physics*, *96*, 3748–3751. https://doi.org/10.1063/1.1778482

Badro, J., Siebert, J., & Nimmo, F. (2016). An early geodynamo driven by exsolution of mantle components from Earth's core. *Nature*, *536*, 326–328. https://doi.org/10.1038/nature18594

Caracas, R. (2015). The influence of hydrogen on the seismic properties of solid iron. *Geophysical Research Letters*, *42*, 3780–3785. https://doi.org/10.1002/2015GL063478

Chi, Z., Nguyen, H., Matsuoka, T., Kagayama, T., Hirao, N., Ohishi, Y., & Shimizu, K. (2011). Cryogenic implementation of charging diamond anvil cells with H_2 and D_2. *Review of Scientific Instruments*, *82*, 105109. https://doi.org/10.1063/1.3652981

Dewaele, A., & Torrent, M. (2013). Equation of state of α-Al_2O_3. *Physical Review B*, *88*, 064107. https://doi.org/10.1103/Physical Review B.88.064107

443 Dewaele, A. S., Loubeyre, P., Occelli, F., Mezouar, M., Dorogokupets, P. I., & Torrent,
444 M. (2006). Quasihydrostatic equation of state of iron above 2 Mbar. *Physical Review*
445 *Letters*, *97*, 215504. https://doi.org/10.1103/Physical Review Letters.97.215504
446 Dorogokupets, P. I., Dymshits, A. M., Litasov, K. D., & Sokolova, T. S. (2017).
447 Thermodynamics and equations of state of iron to 350 GPa and 6000 K. *Scientific*
448 *Reports*, *7*, 41863. https://doi.org/10.1038/srep41863
449 Helffrich, G. (2014). Outer core compositional layering and constraints on core liquid
450 transport properties. *Earth and Planetary Science Letters*, *391*, 256–262.
451 https://doi.org/10.1016/j.epsl.2014.01.039
452 Helffrich, G., Hirose, K., & Nomura, R. (2020). Thermodynamical modeling of liquid Fe-
453 Si-Mg-O: molten magnesium silicate release from the core. *Geophysical Research*
454 *Letters*, *47*, e2020GL089218. https://doi.org/10.1029/2020GL089218
455 Hirao, N., Kawaguchi, S. I., Hirose, K., Shimizu, K., Ohtani, E., & Ohishi, Y. (2020).
456 New developments in high-pressure X-ray diffraction beamline for diamond anvil cell
457 at SPring-8. *Matter and Radiation at Extremes*, *5*, 018403.
458 https://doi.org/10.1063/1.5126038
459 Hirose, K., Tagawa, S., Kuwayama, Y., Sinmyo, R., Morard, G., Ohishi, Y., & Genda, H.
460 (2019). Hydrogen limits carbon in liquid iron. *Geophysical Research Letters*, *46*,
461 5190–5197. https://doi.org/10.1029/2019GL082591
462 Iizuka-Oku, R., Yagi, T., Gotou, H., Okuchi, T., Hattori, T., & Sano-Furukawa, A. (2017).
463 Hydrogenation of iron in the early stage of Earth's evolution. *Nature Communications*,
464 *8*, 14096. https://doi.org/10.1038/ncomms14096
465 Ikuta, D., Ohtani, E., Sano-Furukawa, A., Shibazaki, Y., Terasaki, H., Yuan, L., & Hattori,
466 T. (2019). Interstitial hydrogen atoms in face-centered cubic iron in the Earth's core.
467 *Scientific Reports*, *9*, 7108. https://doi.org/10.1038/s41598-019-43601-z
468 Ohta, K., Ichimaru, K., Einaga, M., Kawaguchi, S., Shimizu, K., Matsuoka, T., et al.
469 (2015). Phase boundary of hot dense fluid hydrogen. *Scientific Reports*, *5*, 16560.
470 https://doi.org/10.1038/srep16560
471 Seto, Y., Nishio-Hamane, D., Nagai, T., & Sata, N. (2010). Development of a software
472 suite on X-ray diffraction experiments. *The Review of High Pressure Science and*
473 *Technology*, *20*, 269–276
474

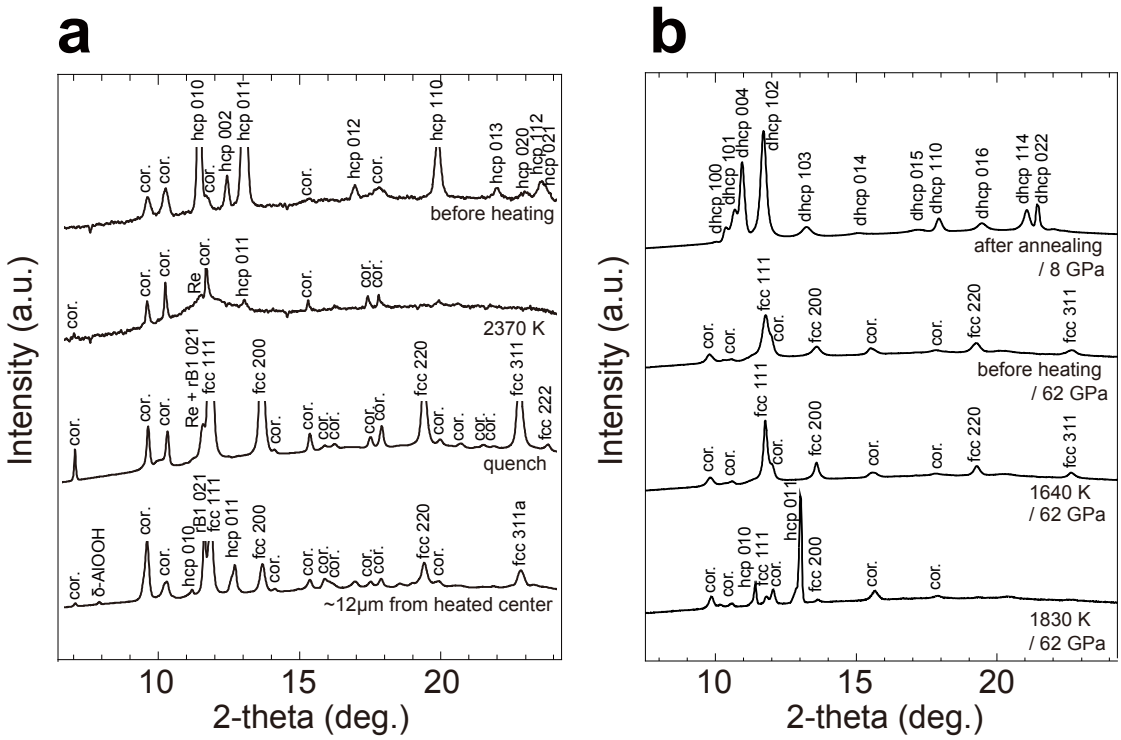

475

476 **Figure 1.** XRD patterns collected in (a) run #A4 for the Fe-O-H sample at ~40 GPa and
477 (b) run #B for the Fe-H sample at ~62 GPa. Hcp, hcp FeH_x.; fcc, fcc FeH_x; dhcp, FeH;
478 rB1, rhombohedral B1 FeO; cor, corundum (pressure medium); Re, rhenium (gasket). In
479 (b), fcc $FeH_{0.77}$ at 1640 K dissociated into hcp $FeH_{0.21}$ and fcc $FeH_{0.69}$ with increasing
480 temperature to 1830 K.

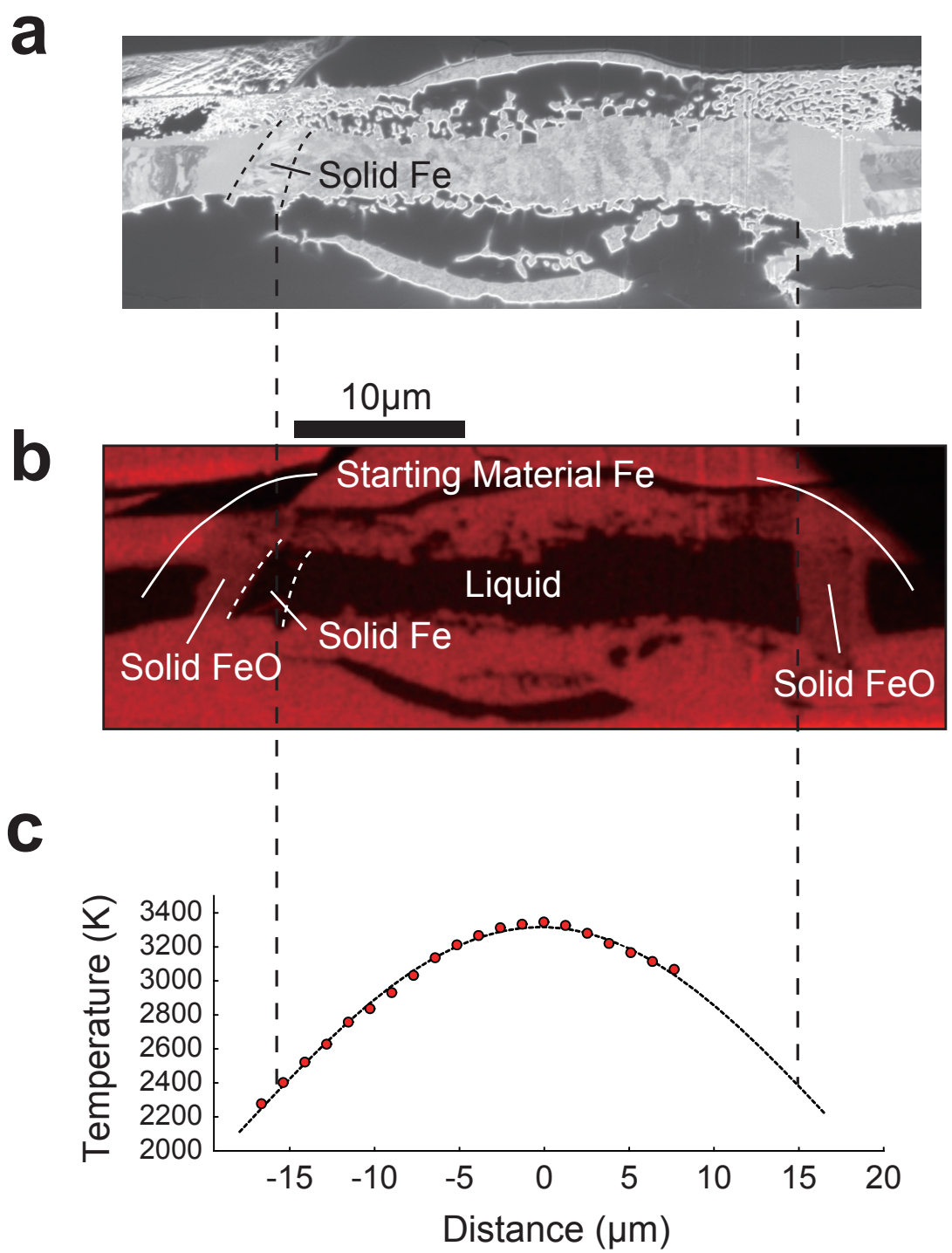

Figure 2. Sample cross sections and temperature profile in run #A4. Scanning ion microscope image (a) and X-ray map of oxygen (b) show that liquid coexisted with solid Fe and FeO. Temperature at the liquid/solid boundary is obtained by a combination of these images and a temperature profile (c).

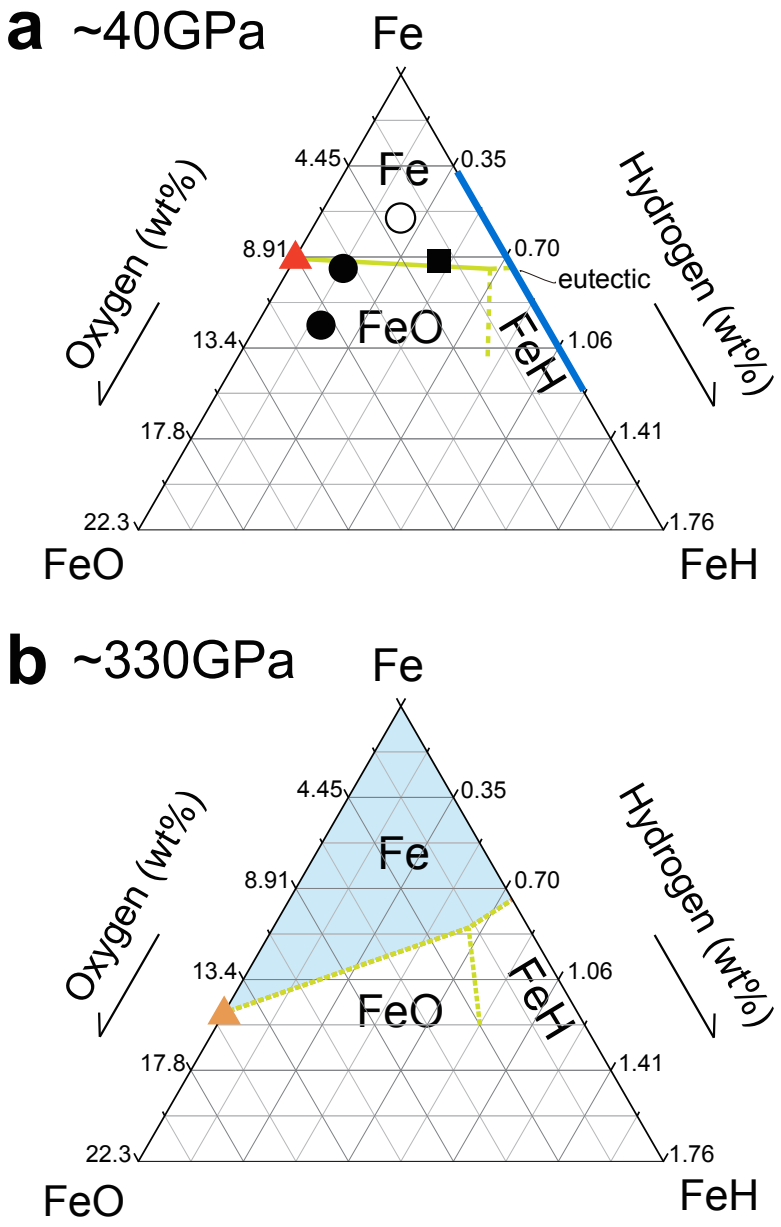

Figure 3. Liquidus phase diagrams of the Fe-FeO-FeH ternary system. Green lines are cotectic lines that separate the liquidus fields of Fe, FeO, and FeH. In (a) for ~40 GPa, circles and square show the compositions of liquids coexisting with FeO and Fe + FeO, respectively (filled and open symbols indicate 0.1–0.4 wt% and 1.7 wt% C in liquids, respectively). A blue bar shows the solid miscibility gap in the Fe-FeH system observed in run #B. The Fe-FeO eutectic liquid composition is given by a red triangle from Figure S1. The Fe-FeH eutectic liquid composition may be $FeH_{0.42}$ (Fe + 0.75 wt% H). (b) The liquidus phase relations extrapolated to 330 GPa considering the Fe-FeO (orange triangle, Figure S1) and Fe-FeH binary eutectic liquid compositions (the latter could exhibit little pressure dependence). The liquidus field of Fe is illustrated by a blue area.

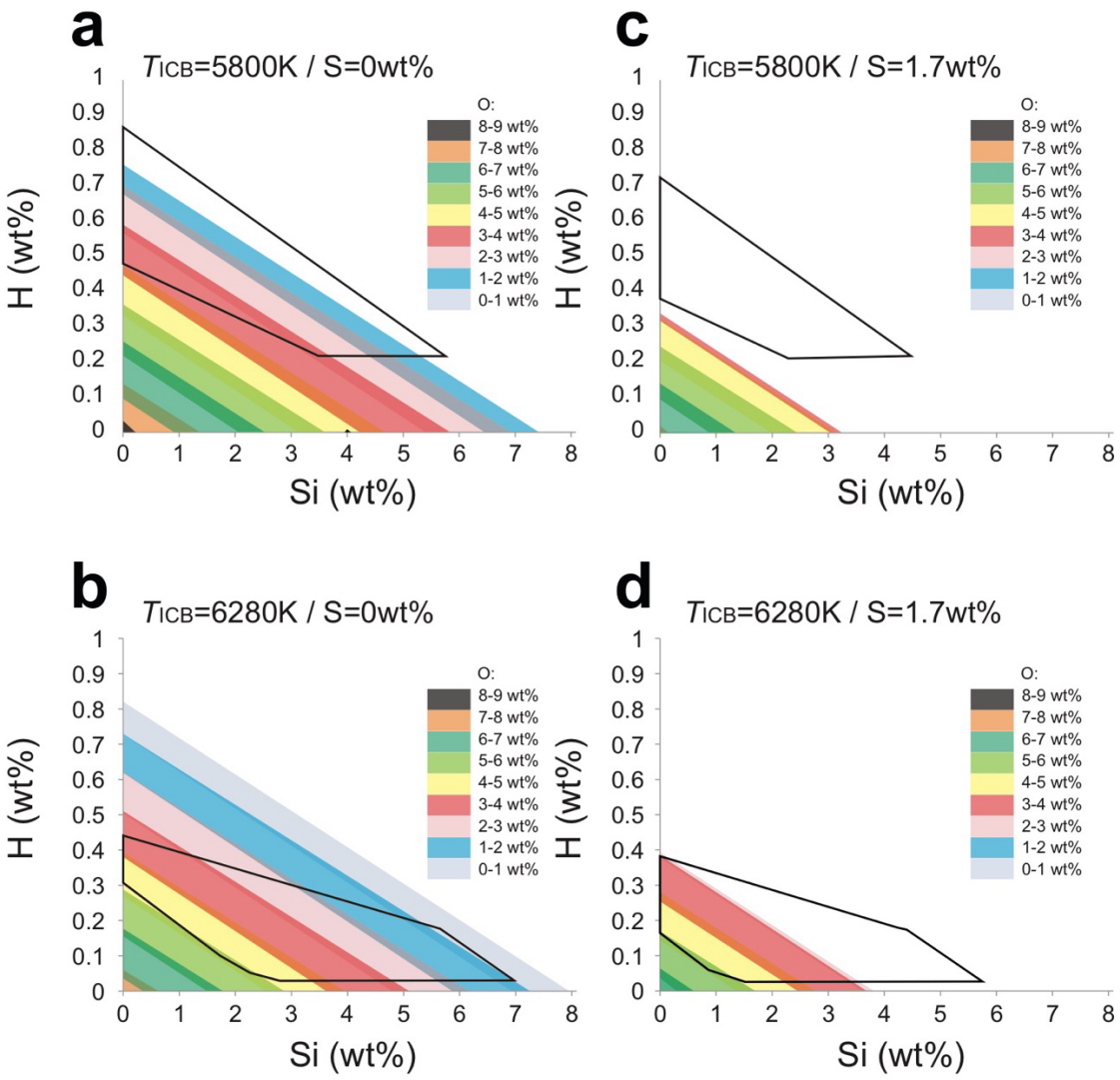

497

498 **Figure 4.** Possible ranges of the outer core liquid composition in the Fe-O-Si-H±1.7wt%S
499 system. Colored areas show liquid compositions that are compatible with the observed
500 outer core density and P-wave velocity (Umemoto & Hirose, 2020) and within the
501 liquidus field of Fe. The areas enclosed by black lines indicate liquid compositions that
502 are in equilibrium with the possible compositions of the inner core solid that explain
503 observed density, P- and S-wave velocities (Li et al., 2018; Wang et al., 2021).
504

Geophysical Research Letters

Supporting Information for

Melting Experiments on Fe-O-H: Evidence for Eutectic Melting in Fe-FeH and Implications for Hydrogen in the Core

Kenta Oka[1], Shoh Tagawa[1,2], Kei Hirose[1,2], and Yasuo Ohishi[3]

[1]Department of Earth and Planetary Science, The University of Tokyo, Bunkyo, Tokyo, Japan

[2]Earth-Life Science Institute, Tokyo Institute of Technology, Meguro, Tokyo, Japan

[3]Japan Synchrotron Radiation Research Institute, SPring-8, Sayo, Hyogo, Japan

Contents of this file

Experimental Methods

Melting experiments on the Fe-O-H system. We used diamond anvils with flat 300 μm or single-beveled 120 μm culet size for experiments on Fe-O±H (Table S1). A pure Fe (5N, *Mairon-UHP*, *Toho Zinc*) or Fe-12wt%O foil, same as that used in Oka et al. (2019), was loaded into a hole at the center of a pre-indented rhenium gasket, together with a powder mixture of $Al(OH)_3$ and Al_2O_3 (a source of oxygen and hydrogen) and 10 μm-thick Al_2O_3 sapphire single crystals (thermal insulation layers). Upon heating, $Al(OH)_3$ dehydrates to form AlOOH or Al_2O_3. The mixing ratio between Al_2O_3 and $Al(OH)_3$ was varied in order to change the Fe/H_2O ratio of a system.

The sample was heated from both sides with a couple of 100W single-mode Yb fiber lasers with flat-top beam-shaping optics. The laser spot size was 20–30 μm across. The heating duration was limited to less than 3 sec to avoid temperature fluctuations which could lead to a complex melting texture. Indeed, it is long enough for O and H to diffuse over a melt pocket (Helffrich, 2014), which assures chemical equilibrium between liquid and solid when considering that melting/crystallization at the liquid-solid boundary occurs almost instantaneously (Yokoo et al., 2019; Hasegawa et al., 2021). According to previous time-series melting experiments on the Fe-S system, the compositions of coexisting liquid and solid did not change after heating for 1 sec in a laser-heated DAC (Mori et al., 2017). The diffusivities of O and H in molten iron are higher than that of S (Helffrich, 2014). A temperature profile was obtained using a spectro-radiometric method (Hirao et al., 2020). The temperature at the liquid/solid boundary corresponds to the liquidus temperature of a liquid obtained in each run. We determined it by combining the temperature profile with a sample cross-section (e.g., Mori et al., 2017; Tateno et al., 2018; Oka et al., 2019) (Figure 2c).

We performed XRD measurements in-situ at high *P*-*T* using an X-ray beam with energy of ~30 keV at the beamline BL10XU, SPring-8 (Figure 1). XRD spectra were collected on a flat panel detector (FPD, *Perkin Elmer*) with exposure time of 1 sec before and after heating at 300 K and of 0.2 sec continuously during laser heating. The IPAnalyzer software (Seto et al., 2010) was used to integrate two-dimensional XRD image into one-dimensional diffraction profile. Sample pressure was measured at 300 K after heating based on the unit-cell volume of Al_2O_3 corundum and its equation of state (Dewaele & Torrent, 2013). We considered that 60% and 90% of theoretical thermal pressure for purely isochoric heating, $\Delta P = \alpha K_T \times (T - 300)$ ($\alpha K_T = 4$ and 9 MPa/K), contributed to an increase in sample pressure during heating at ~40 GPa and ~150 GPa, respectively (e.g., Hirose et al., 2019; Oka et al., 2019).

Textural and chemical characterizations except for H (see below) were carried out on each recovered sample; it is well known that H escapes from metal Fe when it transforms into bcc during decompression (e.g., Iizuka-Oku et al., 2017; Tagawa, Sakamoto et al., 2021). A sample cross-section and X-ray elemental maps were obtained parallel to the compression axis by a focused ion beam (FIB, *FEI Versa 3D DualBeam*) and an energy-dispersive spectroscopy (EDS) attached to a field-emission (FE)-type scanning electron microscope (SEM) (Figures 2a, b). Quantitative chemical analyses were then made for coexisting liquid and crystals (liquidus phases) with an FE-type electron probe micro-analyzer (FE-EPMA, *JEOL JXA-8530F*) with an accelerating voltage of 12 kV, a current of 15 nA, and the X-ray counting time of 20/10 sec for peak/background. Fe, Fe_3C, and corundum were used as standards. LIF (Fe), LDE2H (C), TAP (Al), and LDE1 (O) were analyzing crystals. The FE-EPMA analyses of quenched liquid Fe sometimes included a small amount of Al, which is likely a signal from the surrounding pressure medium or Al_2O_3 grains that mechanically intruded into the liquid; note that the amount of Al incorporated into liquid Fe metal is negligible (Badro et al., 2016; Helffrich et al., 2020). Al was therefore subtracted as Al_2O_3 from raw data. C was detected not only in the quenched liquid but also inside the rhenium gasket; the latter could be due to contamination during FIB and/or FE-EPMA analysis. Thus, we subtracted 0.2–0.4 wt% C from the raw analyses of liquids, which was found on the rhenium gasket in the same sample cross-section. The liquid should have included the remaining 0.1–3.7 wt% C (Table S1).

H concentration, x in FeH_x, was estimated from its lattice volume (Hirose et al., 2019; Tagawa, Sakamoto et al., 2021), which expands proportionally to the H content (Caracas, 2015);

$$x = \frac{V_{FeHx} - V_{Fe}}{\Delta V_H}, \quad (1)$$

where V_{FeHx} and V_{Fe} are the unit-cell volumes of FeH_x and Fe (Dorogokupets et al., 2017 for fcc Fe and Dewaele et al., 2006 for hcp Fe), respectively, and ΔV_H is an increase in the lattice volume of Fe per H atom from Caracas (2015). The error in the H content, x, is estimated to be ±8% at maximum, which is mainly derived from uncertainty in ΔV_H (Ikuta et al., 2019; Tagawa, Sakamoto et al., 2021).

Subsolidus experiment on Fe-H. We have also conducted an experiment on the Fe-FeH binary system (Table S2), using a laser-heated DAC with beveled 200 μm culet anvil. A 10-μm thick pure iron foil was loaded between the disks of Al_2O_3 single crystals. A

whole DAC was dried in a vacuum oven at 393 K for at least one hr and subsequently at 350 K for 30 mins in a vacuumed hydrogen-loading system.

Hydrogen was cryogenically loaded into a sample chamber (Chi et al., 2011). After the chamber was filled with liquid H, sample was compressed at ~15 K and then restored to room temperature. The surface of the diamond anvils was coated with a thin layer of Ti by sputtering (Ohta et al., 2015) in order to avoid anvil failure. FeH_x was synthesized by thermal annealing with a laser at 8 GPa. Upon compression to 23 GPa, excess molecular H_2 in the sample chamber was lost to a neighboring rhenium gasket to form ReH_x (Scheler et al., 2011). We heated the FeH_x sample at 62 GPa with in-situ XRD measurements at BL10XU, SPring-8 (Figure 1b). We obtained pressures of 8 and 23 GPa from the Raman shift of a diamond anvil (Akahama & Kawamura, 2004) and those at 62 GPa based on the lattice volume of Al_2O_3 corundum (Dewaele & Torrent, 2013). Other procedures including the determination of the H contents in solid Fe phases were similar to those for the Fe-O±H sample described above.

606

Table S1

Experimental Results on the Fe-O±H System

Run #	Starting materials	P (GPa) at high T	P (GPa) at 300 K	T (K)	Liquid composition			Liquidus phase
					O (wt%)	H (wt%)	C (wt%)	
A1	Fe-12wt%O + Al_2O_3 + $Al(OH)_3$	35(2)	30(2)	2460(120)	3.53(4)	0.27(2)	1.68(9)	FeO
A2	Fe-12wt%O + Al_2O_3 + $Al(OH)_3$	37(2)	32(2)	2470(110)	7.20(4)	0.18(1)	0.11(9)	FeO
A3	Fe-12wt%O + Al_2O_3 + $Al(OH)_3$	41(2)	36(2)	2400(120)	9.53(18)	0.22(2)	0.20(12)	FeO
A4	Fe + $Al(OH)_3$	39(2)	33(2)	2370(120)	2.98(29)	0.49(4)	0.43(4)	Fe[d] + FeO
A5	Fe + Al_2O_3 + $Al(OH)_3$[c]	147(15)	122(12)	3200(320)	12.97(86)	0.00(0)	0.86(7)	Fe
A6	Fe + Al_2O_3 + $Al(OH)_3$[c]	160(16)	136(14)	3200(320)	10.36(56)	0.04(0)	3.74(23)	FeO

[a] Al_2O_3 : $Al(OH)_3$ = 10 : 3 by weight

[b] Al_2O_3 : $Al(OH)_3$ = 10 : 4 by weight

[c] Al_2O_3 : $Al(OH)_3$ = 10 : 8 by weight

607 [d] contains 0.43(3) wt% H

608

609

610

611

612

Table S2

Experimental Results on the Fe-H System

Run #	P (GPa)	T (K)	hcp FeHx				fcc FeHx			dhcp FeHx			
			a (Å)	c (Å)	V (Å^3)	x	a (Å)	V (Å^3)	x	a (Å)	c (Å)	V (Å^3)	x
B	8(1)	300								2.656(1)	8.691(10)	53.08(23)	1.00(6)
	44(4)	300					3.539(1)	44.34(8)	0.87(5)				
	62(6)	1640(70)					3.498(1)	42.80(5)	0.77(5)				
	62(6)	1830(80)	2.393(5)	3.919(14)	19.44(36)	0.21(1)	3.487(1)	42.41(9)	0.69(4)				

613

614

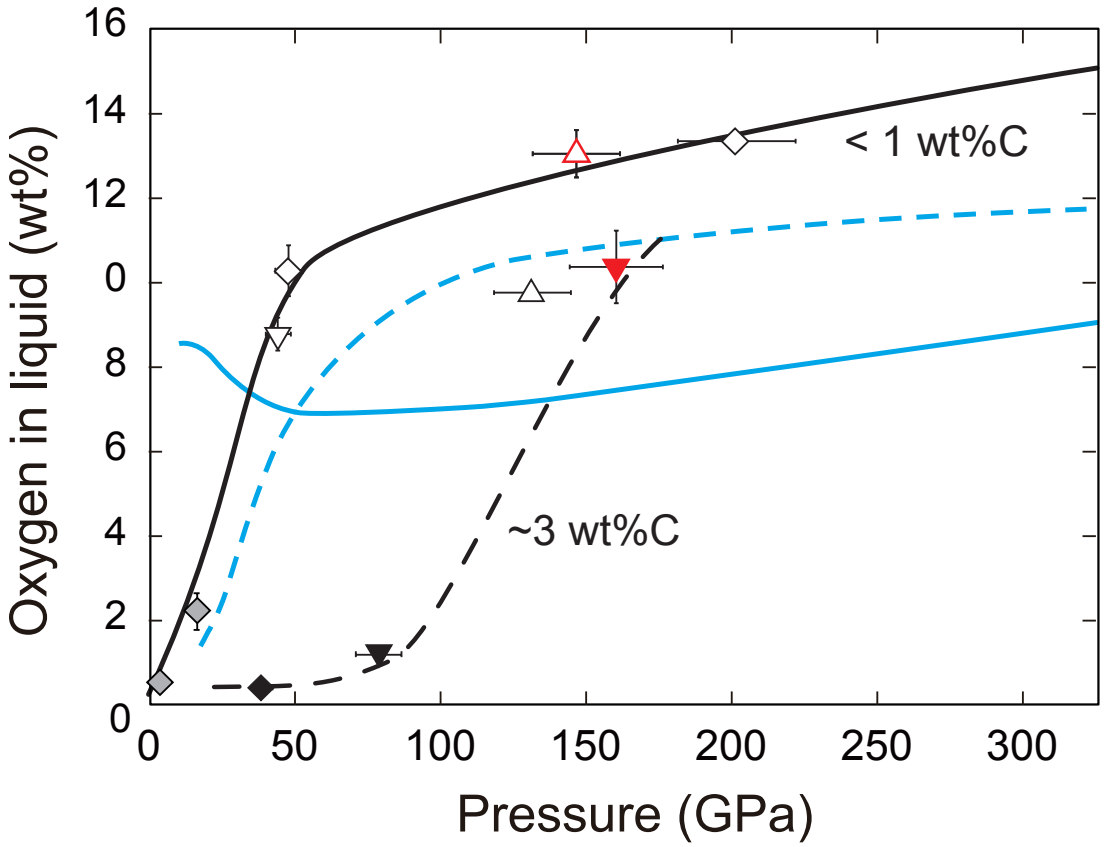

Figure S1. Liquid compositions obtained in melting experiments on the Fe-FeO±C system. Normal and reverse triangles, lower and upper bounds for O concentration in the Fe-FeO eutectic liquid, respectively; diamonds, the O contents in liquids coexisting both Fe and FeO (eutectic liquids). Red, this study (runs #A5 and #A6); black, Oka et al. (2019); gray, Ohtani et al. (1984) and Ringwood & Hibberson (1990). The black curves indicate changes in O concentration in liquids coexisting with Fe and FeO (solid line, with <1 wt% C in liquids; broken line, with ~3 wt% C in liquids). Blue dashed and solid curves represent thermodynamically-modelled eutectic liquid compositions in the Fe-FeO system assuming non-ideal and ideal solutions, respectively (Komabayashi, 2014).